MOLECULAR AND CELLULAR BIOLOGY, Sept. 2009, p. 5046–5059 Vol. 29, No. 18
0270-7306/09/$08.00+0 doi:10.1128/MCB.00315-09

The Absence of Caveolin-1 Increases Proliferation and Anchorage-Independent Growth by a Rac-Dependent, Erk-Independent Mechanism▽

Ana Cerezo,[1]† Marta C. Guadamillas,[1]† Jacky G. Goetz,[1] Sara Sánchez-Perales,[1] Eric Klein,[2] Richard K. Assoian,[2] and Miguel A. del Pozo[1]*

Integrin Signaling Laboratory, Department of Vascular Biology and Inflammation, Centro Nacional de Investigaciones Cardiovasculares, Melchor Fernández Almagro 3, 28029 Madrid, Spain,[1] and Department of Pharmacology, University of Pennsylvania School of Medicine, Philadelphia, Pennsylvania 19104-6084[2]

Received 11 March 2009/Returned for modification 18 April 2009/Accepted 10 July 2009

Anchorage-independent growth (AIG) of cancer cells requires escape from integrin-mediated signals. A protein frequently downregulated in cancer, caveolin-1 (Cav1), mediates integrin control of several growth-regulatory pathways. We report that loss of Cav1 results in faster exit from quiescence and progress through the cell cycle, proliferation without anchorage to substrate, and absence of cyclin D1 downregulation upon serum deprivation or detachment. Surprisingly, this proliferative advantage is independent of Erk–mitogen-activated protein kinase signaling; instead, cyclin expression and cell cycle progression in the absence of Cav1 are driven by increased membrane order and Rac targeting. AIG was induced in Cav1-expressing cells by forced membrane targeting of Rac1 or by inhibiting Cav1-mediated internalization of plasma membrane ordered domains at which Rac1 accumulates. Restoring Rho activity, which is downregulated after loss of Cav1, antagonizes Rac1 and prevents cyclin D1 accumulation after serum starvation or loss of adhesion. Anchorage independence and increased proliferation in Cav1-deficient tumoral and null cells are thus due to an increased fraction of active Rac1 at membrane ordered domains. These results provide insight into the mechanisms regulating growth of cancer cells, which frequently lose Cav1 function.

Proliferation of most nontransformed cells requires signals from growth factor receptors and proper anchorage to substrate (1). Anchorage is sensed by integrins, which are the major receptors of the extracellular matrix (ECM) and regulate most signaling cascades linked to cell proliferation, including the Erk–mitogen-activated protein kinase (MAPK), Src, phosphatidylinositol 3-kinase (PI3K), focal adhesion kinase, and Rho GTPase pathways. Coordination of signals from growth factor receptor tyrosine kinases and ECM receptors allows anchorage-dependent proliferation (1, 4, 38, 49). Detachment from substrate terminates integrin-driven signals, leading to cell cycle arrest and/or apoptosis (19). Occasionally, certain cells can escape integrin control of proliferation, a feature known as anchorage-independent growth (AIG) and a characteristic of most transformed cells (18).

Cell cycle progression is driven by sequential activation of specific cyclin-dependent kinase (cdk) complexes. During G_1, activated cyclin D-cdk4/6 and cyclin E-cdk2 phosphorylate retinoblastoma protein (pRb) and the other pocket family proteins, p130 (Rb2) and p107 (7, 50). Phosphorylated pRb allows release of transcription factors critical for G_1-S transition. Induction of cyclin D (and thus activation of cdk4/6) is the initiator step for exit from quiescence and progression through G_1 and eventually the whole cell cycle, since the other phases (S, G_2, and M) are independent of growth factors and adhesion; conversely, specific knockdown of cyclin D1 inhibits entry into S phase (57).

Rho family small GTPases are important integrators of signals from integrins and growth factor receptors, and altered Rho GTPase signaling is related to cell transformation, tumor invasion, and metastasis (2, 4, 5, 46). In particular, Rac1 can drive cyclin D1 transcription in response to integrin signals and growth factors by activating Jun N-terminal protein kinase, PI3K, NF-κB, or MAPK signaling cascades and also contributes to cyclin D1 translation and pRb phosphorylation (41, 45). RhoA and Rac1 coordinately regulate the timing of cyclin D1 expression: while Rac signaling allows cyclin D1 expression in G_0 and early G_1 (which is normally antagonized by Rho), expression in mid-G_1 requires a Rho-dependent sustained activation of Erk proteins (59). Thus, a precise balance in the activities of these GTPases is necessary for correct timing of cyclin D1 expression and subsequent cell cycle progression.

Integrin signals target Rho GTPases and other signaling intermediates to cholesterol-enriched membrane microdomains (CEMMs) (reviewed in references 27 and 30), where they interact with downstream effectors (9). Integrin uncoupling by detachment from the ECM results in CEMM internalization and termination of associated signaling (9). Caveolae are a flask-shaped CEMM subtype characterized principally by the abundance of caveolin proteins, which are essential for caveola formation (40, 43). Cav1 actively participates in CEMM endocytosis after cell detachment, shutting down caveola/CEMM-associated signals (10, 43). Cav1-deficient cells therefore cannot internalize CEMMs upon detachment,

* Corresponding author. Mailing address: Integrin Signaling Laboratory, Department of Vascular Biology and Inflammation, Centro Nacional de Investigaciones Cardiovasculares, Melchor Fernández Almagro 3, 28029 Madrid, Spain. Phone: 34 914531212. Fax: 34 914531265. E-mail: madelpozo@cnic.es.
† These authors contributed equally to this work.
▽ Published ahead of print on 20 July 2009.

even though general CEMM composition is not greatly altered (15). As a result, detached Cav1$^{-/-}$ mouse embryonic fibroblasts (MEFs) show increased Ras-MAPK, PI3K-Akt, and Rac–p21-activated kinase (PAK) signaling (10); all of these signal paths are important for cell cycle progression.

Because many of the signaling molecules located at CEMMs are important for the cell cycle, it is likely that deregulation of Cav1 expression is relevant for cell proliferation. Indeed, Cav1-deficient cells are hyperproliferative, and knockout animals show hypertrophy and hyperplasia in several tissues and organs and increased cell proliferation (36). This is often associated with hyperactivation of MAPK signaling (62). Since the Ras-Erk pathway is a critical regulator of cell cycle progression, it has been proposed that this cascade is responsible for the hyperproliferative phenotype of Cav1-deficient cells, although this question has not been directly addressed so far.

The role of Cav1 in tumor onset and progression is controversial (22). Loss of Cav1 expression contributes to tumorigenesis in several models (36). Genes encoding Cav1 and -2 are located on a putative tumor suppressor locus (17). In fact, 16% of human breast cancers present a P132L mutation in Cav1 (28, 61), and other Cav1 mutations are found in human oral squamous cell carcinomas (26). Many oncogenes, including the *Src*, *Ras*, and *Bcr-Abl* oncogenes, transcriptionally downregulate Cav1 expression (34, 60). Therefore it was proposed that Cav1 could act as a tumor suppressor, and several studies suggest a connection between loss of Cav1 expression and the ability of cells to escape from anchorage growth control (reviewed in references 22, 43, 47, and 62). However, for some tumors, including non-small cell lung cancer, prostate cancer, and some types of breast cancer, Cav1 expression contributes to cell survival and growth, favoring tumor progression (52, 55, 63). Thus, depending on the tumor origin, Cav1 might act either as a tumor suppressor or as a tumor promoter. The molecular mechanisms underlying these cell-type-specific growth-regulatory behaviors are unknown, and the mechanism by which Cav1 regulates anchorage-dependent cell growth remains poorly understood.

In this study we have analyzed the proliferative response of cells deficient in Cav1 expression (by either genetic deletion or tumoral downregulation) to mitogenic stimuli and loss of adhesion. We have found that Cav1-deficient fibroblasts show a faster exit from quiescence and progression through the cell cycle, consistent with the potential role of Cav1 as a tumor suppressor. Furthermore, Cav1-negative cells proliferate in the absence of substrate anchorage, suggesting that loss of Cav1 regulation is an important step in the acquisition of the transformed phenotype. Contrary to what was expected based on previous studies with antisense-mediated inhibition or deletion of Cav1 in cells (20, 44), the proliferative advantage acquired by the loss of Cav1 appears to be independent of the Erk-MAPK pathway. Our results suggest that, instead, proper membrane trafficking and Rac1 plasma membrane targeting play a pivotal role in the regulation of cell proliferation mediated by integrins and Cav1. These studies suggest connections between plasma membrane organization and signals that regulate the cell cycle and will likely contribute to a better understanding of the role of adhesive signaling and Cav1 in the regulation of anchorage dependency of cell proliferation and tumor suppression.

MATERIALS AND METHODS

Handling of mice. Cav1-deficient mice, strain Cav-1 tm1Mls/J, and their wild-type (wt) controls, strain B6129SF2/J, were obtained from The Jackson Laboratory (Bar Harbor, ME). Mice were maintained according to the animal care standards established by the European Union.

Cell culture assays. Primary MEFs were isolated from embryonic day 13.5 embryos. 3T3 immortalized MEFs (MEFs-D and MEFs-R, derived from two mouse strains [15, 44]) and thymus fibroblasts (TFs) (56) from wt and Cav1$^{-/-}$ littermate mice were used throughout this study. When the cell type is not stated, MEFs-R were used. 3T3L1 preadipocytes stably expressing small interfering RNA (siRNA) for Cav1 or a scramble siRNA were generated by lentiviral infection (24). Cav1$^{-/-}$ MEFs and TFs reconstituted with Cav1 (RC MEFs and RC TFs) and M21L-Cav1 melanoma cells were generated by stable transfection of Cav1$^{-/-}$ cells with a Cav1-encoding vector. MEFs and 3T3L1 fibroblasts were cultured in Dulbecco's modified Eagle medium (DMEM) supplemented with 10% fetal bovine serum (FBS), 100 U/ml penicillin, and 100 μg/ml streptomycin at 37°C in a humidified 5% CO_2-95% air incubator. For M21L-Cav1 cells 0.5 mg/ml G418 was added to the culture medium (10). Rat1 fibroblasts expressing myc-tagged V12 Rac (Rat1-V12Rac) or an empty vector (Rat1-V8) were cultured in DMEM with 10% FBS, 0.5 mg/ml G418, and 2 μg/ml doxycycline (11). For experiments with nonadhered cells, cells were plated on bacterial plastic dishes coated with a thin layer of 0.5% agarose and cultured for 18 h; alternatively, for bromodeoxyuridine (BrdU) incorporation and CEMM retention assays cells were grown under permanent rotation in DMEM containing 0.5% methylcellulose and 2 μM HEPES. In both cases nonadhered cultures were grown in the presence of 10% FBS. Specific inhibitors of PI3K (50 μM LY294002) and glycogen synthase kinase 3β (GSK3β) (40 mM LiCl) were added to the culture plates for 18 h. To analyze S-phase entry, cells were serum deprived for 72 h in DMEM plus 0.1% FBS and then restimulated with 10% FBS to trigger cell cycle reentry. DNA content was analyzed by flow cytometry after propidium iodide staining (FACs Canto II flow cytometer; BD). G_0/G_1, S, and G_2/M cell cycle phases were quantified with FACs Diva software. BrdU incorporation was measured by indirect immunofluorescence after 2 or 5 h in the presence of 50 μM BrdU. For focus formation assays 5×10^5 wt and Cav1$^{-/-}$ immortal MEFs were cotransfected with a plasmid containing the human H-Ras oncogene and a green fluorescent protein (GFP)-expressing plasmid to assess efficiency of transfection and allowed to grow for 10 days, until visible colonies formed. Foci were stained with 0.05% crystal violet solution for 1 h. Primary MEFs were transfected with a plasmid containing the H-Ras oncogene either alone or with a plasmid containing the E1A oncogene. For soft agar assays 1.5×10^4 cells were resuspended in 3 ml of complete medium containing 0.35% agarose. The mixture was seeded on a layer of medium containing 0.5% agarose. Cells were allowed to reach interphase at 37°C for 20 min. After solidification, 2 ml complete medium was added. Cells were grown at 37°C and 5% CO_2 for 3 weeks. Colonies were stained with 0.005% crystal violet for 1 h.

Antibodies and reagents. The specific primary antibodies used were anti-cyclin D1 monoclonal antibody (MAb) (sc-8396; Santa Cruz Biotechnology, Inc.), anti-cyclin A polyclonal antibody (PAb) (sc-751; Santa Cruz Biotechnology, Inc.), anti-γ-tubulin MAb (T6557; Sigma-Aldrich), anti-pRb MAb (554136; BD Pharmingen), anti-p-pRb (pS807/811) PAb (9308; Cell Signaling), anti-p107 PAb (ab2451-1; Abcam), anti-p130 PAb (ab6545-100; Abcam), anti-p-Erk (pTpY185/187) PAb (44-680G; Biosource International), anti-Erk1 and -2 pan-PAb (44-654G; Biosource International), anti-myc MAb (clone 9E10, sc-40; Santa Cruz), anti-cdk4 MAb (sc-260; Santa Cruz), anti-Rac MAb (05-389; Upstate Biotechnology), anti-p-Akt (pS473) MAb (44-621G; Biosource International), anti-p-Akt (pT308) PAb (9275; Cell Signaling), anti-Akt PAb (9272; Cell Signaling Technology), antihemagglutinin (anti-HA) MAb (MMS-101P; Covance), and anti-BrdU MAb Alexa Fluor 594 conjugate (A21304; Molecular Probes). Alexa Fluor 488 (A11001) antibodies and Alexa Fluor 647 phalloidin (A22287) were purchased from Molecular Probes, and peroxidase-conjugated goat anti-rabbit and anti-mouse immunoglobulin G were obtained from Jackson ImmunoResearch Laboratories, Inc. The inhibitors used were LY294002 (440202; Calbiochem), U0126 (662005; Calbiochem), and LiCl (Sigma-Aldrich).

Rac pulldown assay and Western blot analysis. Rac activity in starved MEFs was determined by pulldown assay as described previously (11). For Western blotting, cells were lysed in modified radioimmunoprecipitation assay buffer containing 50 mM Tris-HCl (pH 7.4); 1% NP-40; 0.1% sodium dodecyl sulfate; 0.25% Na deoxycholate; 150 mM NaCl; 1 mM EDTA; 1 mM EGTA; 1 mM phenylmethylsulfonyl sulfate; 1 μg/ml each of aprotinin, leupeptin, and pepstatin; and 25 mM NaF (all from Sigma). Equal amounts of protein were resolved by sodium dodecyl sulfate-polyacrylamide gel electrophoresis. Proteins were transferred to nitrocellulose membranes (Amersham) and probed with antibod-

ies using standard procedures. Horseradish peroxidase-bound antibodies were detected by chemiluminescence with ECL (Amersham Life Sciences, Little Chalfont, United Kingdom). Densitometric analysis of bands was performed with Quantity One software (Bio-Rad). Electrophoretic mobility of pocket proteins was analyzed using the Leica LAS-AF software.

DNA constructs and transient transfection assays. Vectors encoding enhanced GFP (EGFP)-Cav1, EGFP-Rac T17N (12), myr-HA-Rac, and interleukin-2 (IL-2)–HA–Rac (11) were transiently transfected by electroporation. The GFP-positive population was separated 24 h later with a MoFlo cell sorter (Dako-Cytomation).

Adenoviral infection. MEFs were infected with LacZ (control) or N17-Rac adenovirus at a multiplicity of infection of 300 as described previously (33). N17-Rac adenovirus was a generous gift from Anne Ridley (Ludwig Institute for Cancer Research, University College London, United Kingdom).

qPCR. Total RNA was collected and analyzed by quantitative PCR (qPCR) using TaqMan primer and probe sequences for mouse cyclin D1 mRNA and cdk4 mRNA as described previously (33). qPCR results show levels of cyclin D1 mRNA normalized to those of cdk4 and are plotted as means ± standard deviations of duplicate PCRs. The levels of cdk4 mRNA were not affected by the culture conditions or treatments.

CEMM retention assays. Latex beads were coated with anti-transferrin receptor (anti-TfR) antibody or cholera toxin B (CTxB) as previously described (9). Cells were incubated with coated beads at a cell-to-bead ratio of 1:40 for 1 h and then placed in suspension for 12 h. BrdU (50 μM) was added 5 h before collection of the cells.

RNA interference (RNAi)-mediated silencing. Small interfering RNA (siRNA) transfections targeting Akt and Rac proteins were performed 24 h before transfer of Cav1$^{-/-}$ cells to suspension culture using Oligofectamine (Invitrogen) and a 100 nM Akt target sequence (5′-CCTGCCCTTCTACAACCAGGA-3′) (37) (Ambion), a 100 nM mRac1 target sequence (5′-CAGACAGACGUGUUCUU AAUUUGCU-3′) (31), or a 100 nM scrambled siRNA oligonucleotide as a control (both from Invitrogen). For GSK3β, a mU6pro vector carrying the specific short hairpin RNA (shRNA) sequence 5′-TAAGAACCGAGAGCTCC AGATC-3′ (64) or an empty vector was transiently electroporated into wt MEFs 24 h before transfer of cells to suspension.

Immunofluorescence labeling and confocal microscopy. Cells grown on glass coverslips were fixed in 4% paraformaldehyde for 15 min at room temperature. Cells were grown in suspension for 16 h, fixed with 4% paraformaldehyde, washed with phosphate-buffered saline (PBS), and placed on slides by centrifugation at 1,000 rpm for 1 h (Shandon Cytospin 4; Thermo). After fixation, cells were rinsed extensively with PBS and permeabilized with 0.1% Triton X-100 in PBS containing 1% bovine serum albumin for 15 min to reduce nonspecific binding. For BrdU staining, an additional step of denaturation with 2 N HCl for 25 min was performed. Subsequent washing and incubations with phalloidin and primary and fluorescent secondary antibodies were done in PBS containing 0.2% bovine serum albumin. After labeling, coverslips were mounted in Permafluor aqueous mounting medium (IM0752; Immunotech/Beckman Coulter) and analyzed with the 63× and 40× objectives of a Leica SPE confocal microscope. To quantify cyclin D1 nuclear accumulation, nuclei were delimited by Hoechst labeling and the intensity of cyclin D1 immunostaining was quantified with Leica LAS-AF software. A minimum of six fields were acquired per condition, and 30 to 50 cells per condition were quantified ($n = 3$). To quantify plasma membrane localization of myr-Rac and IL-2–Rac, 10 line profiles per cell (5 to 6 μm) were obtained and quantified with Leica LAS-AF software (using either the Rac or HA labeling).

Statistical analysis. Statistical significance was determined by a two-tailed Student t test with Prism 4.0 software (GraphPad Software, Inc., San Diego, CA). P values that were <0.05 were considered significant.

RESULTS

Loss of Cav1 accelerates proliferation and cooperates in oncogenic transformation. Cav1-deficient fibroblasts cycle faster and have a larger S-phase fraction than wt cells, as shown by flow cytometric analysis and BrdU incorporation (15, 44) (Fig. 1a). We observed that the levels of cyclins D1 and A, which are characteristic of G_1 and S/G_2, respectively, were elevated in Cav1$^{-/-}$ MEFs and in Cav1-silenced 3T3L1 cells and that pRb phosphorylation was higher (Fig. 1b). Cyclin D1 accumulation in Cav1$^{-/-}$ MEFs was predominantly nuclear (Fig. 1c). Expression of p130, an early G_1 marker (6), was also lower in Cav1$^{-/-}$ cells, whereas expression of the late G_1 marker p107 was higher (Fig. 1b). Increased cyclin D1 and a reduced G_0/G_1 population in Cav1-deficient cells from three different knockout mouse models (15, 44, 56) and Cav1-silenced 3T3L1 cells were observed (Fig. 1a; data not shown). Restoration of Cav1 expression rescued the wt phenotype in all cases (Fig. 1d). Also, Cav1 reexpression in the M21L melanoma tumor cell line (M21L-Cav1), which does not otherwise express Cav1, resulted in an increased G_0/G_1 (Fig. 1e). Lack of Cav1 thus seems to increase the proportion of cells in late versus early G_1, as well as in S and G_2/M, perhaps indicating faster progression through G_1. Cav1$^{-/-}$ mice are prone to tumor development, and Cav1 deficiency cooperates with oncogenes in MEF cell transformation in an INK4a-deficient background (22, 47, 62). We found that immortal Cav1$^{-/-}$ MEFs transfected with the H-Ras oncogene formed up to 10-fold more oncogenic foci than control cells (Fig. 2a). Moreover, H-Ras expression alone was sufficient to produce foci in primary MEFs deficient for Cav1 (Fig. 2b), confirming that lack of Cav1 promotes focus formation, one of the features of cell transformation.

Cav1-deficient cells progress faster through cell cycle. To analyze the effects of Cav1 deficiency in synchronized cultures, we arrested wt and Cav1$^{-/-}$ MEF-R and TF populations at G_0 by depleting serum (shown for MEFs-R in Fig. 3a). wt cells began to exit G_0/G_1 16 h after serum readdition, correlating with an increased fraction of cells in S phase. Over 24 h, the G_0/G_1 population declined from 86% ± 2.8% to 49% ± 3.4%, while the S and G_2/M fractions reached 29% ± 2.4% and 21% ± 5.3%, respectively. Cav1$^{-/-}$ cells began G_0/G_1 exit 12 h after serum readdition, and after 16 h the S and G_2/M populations were 30% ± 4.7% and 17% ± 5.1%, respectively. The S-phase population began to decline from 20 h, while the G_2/M population reached 34% ± 4.7%. The increase in the Cav1$^{-/-}$ G_0/G_1 population at 24 h corresponds to entry into a second cycle. These differences were reflected in the expression of cyclins and pocket family proteins (Fig. 3b). Cyclin D1 began to accumulate in wt MEFs 8 h after serum readdition, peaking at 16 h, just before cells enter S phase. Increased entry into S phase (20 h) was mirrored by decreased levels of cyclin D1, whereas the levels of cyclin A continued to increase. Phosphorylation of pRb and p130 was detected at 12 h and 4 h, respectively, and p107 levels increased progressively as cells left G_0 and progressed through G_1 and S phases. Strikingly, cyclin D1 was highly expressed in serum-starved Cav1$^{-/-}$ cells (both MEFs-R and TFs); this expression increased slightly after 8 h of serum stimulation and did not decline until 16 h, correlating with the sharp increase in the S-phase population (shown for MEFs-R in Fig. 3a) and presumably due to proteasomal degradation (13). Again, cyclin D1 accumulation in Cav1$^{-/-}$ MEFs was predominantly nuclear (Fig. 3c). The increase in cyclin A levels upon serum readdition was higher in Cav1$^{-/-}$ cells, and maximal levels of cyclin A and phosphorylated pRb were reached 20 h after serum stimulation, coinciding with the minimum G_1 and maximum S and G_2/M fractions (Fig. 3a). Cyclin A expression in Cav1$^{-/-}$ cells decreased again at 24 h, coinciding with entry into the next cycle (not shown). The timing of pRb phosphorylation was little affected by Cav1 deficiency, but protein expression of pRb and p130 pocket proteins was low, probably contributing to the faster progression

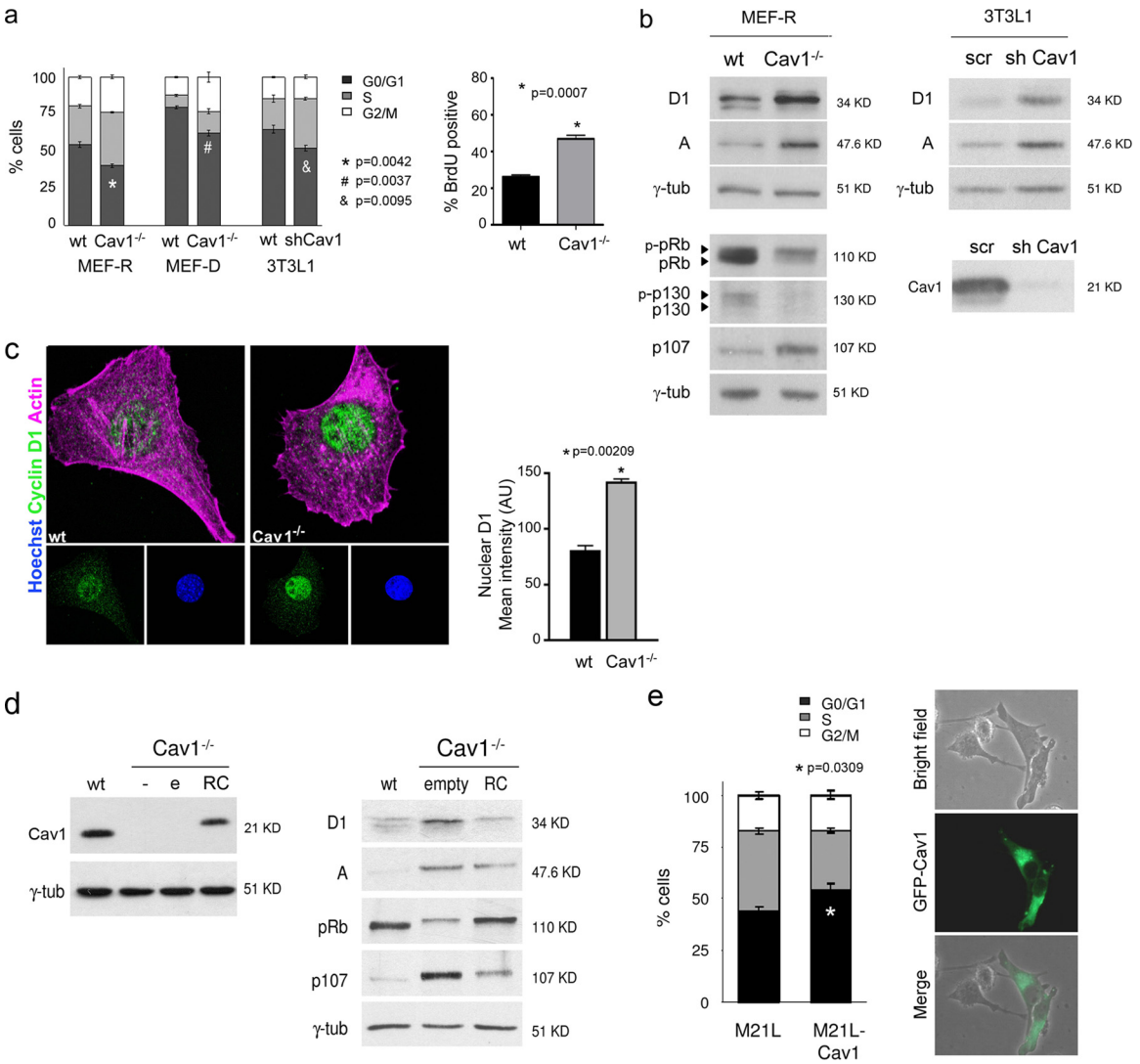

FIG. 1. Increased cell proliferation in the absence of Cav1. (a) Flow cytometric analysis of wt and Cav1$^{-/-}$ MEFs from two different mouse strains (MEF-R [44] and MEF-D [15]) and 3T3L1 fibroblasts before and after shRNA-mediated Cav1 knockdown, showing the percentages of cells in each phase of the cell cycle out of a total of 10,000 cells (left), and analysis of BrdU incorporation after 2-h labeling of wt and Cav1$^{-/-}$ MEFs-R (right). (b) Western blot analysis of wt and Cav1$^{-/-}$ MEFs-R using antibodies against cyclin D1, cyclin A, pRb, p130, p107, and γ-tubulin (γ-tub; as a loading control) (left) and Western blot analysis of 3T3L1 fibroblasts before and after Cav1 shRNA-mediated specific knockdown using antibodies against cyclin D1, cyclin A, Cav1, and γ-tubulin (as a loading control) (right). (c) Immunofluorescence staining of wt and Cav1$^{-/-}$ MEFs-R using an antibody against cyclin D1 and phalloidin to visualize the actin cytoskeleton. Nuclear cyclin D1 mean intensity is represented. At least 30 cells per genotype were analyzed. AU, arbitrary units. (d) Western blot analysis of wt and Cav1$^{-/-}$ MEFs-R expressing either an empty vector (e) or Cav1 (RC) using antibodies against Cav1, cyclin D1, cyclin A, pRb, and p107. γ-Tubulin was used as a loading control. (e) Flow cytometry analysis of M21L cells expressing either an empty vector or a construct encoding GFP-fused Cav1, showing the percentages of cells in each phase of the cell cycle out of a total of 10,000 cells (left), and GFP-Cav1 expression in adherent M21L melanoma cells (right). Bars (a, c, and e) represent means ± standard errors of the means of three (a and c) or four (e) independent experiments.

through G_1 (Fig. 3b and d). Conversely, the increase in p107 levels upon serum stimulation was stronger in Cav1$^{-/-}$ cells (15-fold versus 4-fold in wt cells at 20 h). To determine whether Cav1$^{-/-}$ cells withdraw from the cell cycle and enter G_0 or are arrested at early G_1, we analyzed the phosphorylation status of pRb protein at residues specifically targeted by the cdk4/6-cyclin D1 complex (S807/811). p-pRb (pS807/811) was undetectable in serum-starved wt and Cav1$^{-/-}$ MEFs, and cells of both genotypes showed the same rate of induction upon serum addition (Fig. 3e). We also analyzed the nuclear accumulation of the transcription factor Fox03a after serum starvation, an indicator of G_0 arrest (39). wt and Cav1$^{-/-}$ MEFs showed similar levels of nuclear accumulation of Fox03a after serum starvation and the same rate of nuclear exclusion 30 min and 1 h after serum addition (not shown). These results suggest that Cav1$^{-/-}$ MEFs arrest at G_0 as efficiently as wt MEFs after serum starvation and that the timing of G_0 exit by Cav1$^{-/-}$ MEFs does not differ from that for wt MEFs. Thus, Cav1-deficient cells apparently reenter the cell cycle at the same rate as wt MEFs but progress faster through G_1, completing this phase ~4 h earlier.

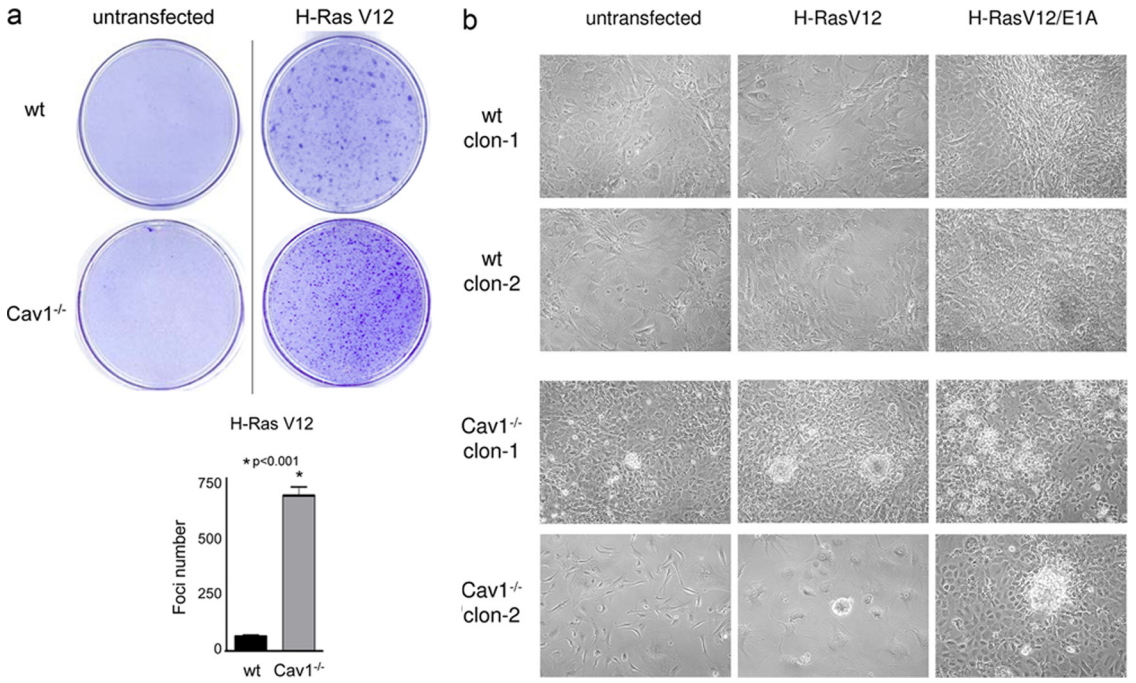

FIG. 2. Cav1 deficiency cooperates in oncogenic transformation of MEFs. (a) Focus formation assay of wt and Cav1$^{-/-}$ MEFs-R after transfection with the H-Ras oncogene. Total foci formed normalized to wt cells are represented. The ratios of focus formation in transfected cells were 1/1,000 for wt cells and 1/100 for transfected Cav1$^{-/-}$ cells. Bars represent means ± standard errors of the means of four independent experiments. (b) Micrographs showing focus formation in two independent primary clones (clon) of wt and Cav1$^{-/-}$ MEFs-R, respectively, after transfection with the H-Ras oncogene or the H-Ras and E1A oncogenes.

Cyclin D1 accumulation in Cav1-deficient cells is Erk independent but Rac dependent. Sustained Erk activation is required for serum-induced cyclin D1 expression and is modulated by Rho GTPases (59). Since it has been suggested that Erk hyperactivation accounts for the hyperproliferative phenotype of Cav1$^{-/-}$ animals, we examined whether this pathway mediates cyclin D1 accumulation in G_0. Pretreatment of synchronized Cav1$^{-/-}$ MEFs with the MEK inhibitor U0126 did not affect cyclin D1 expression (Fig. 4a), indicating that cyclin D1 accumulation in Cav1$^{-/-}$ cells is independent of MAPK activation.

Cyclin D1 expression is also regulated by the GTPase Rac (41, 45). We previously showed that Rac activity in asynchronous Cav1$^{-/-}$ MEF cultures is enhanced 1.5-fold compared with that in wt cultures (25), and this was increased to almost 5-fold in G_0-synchronized cultures (Fig. 4b). Suppression of Rac with dominant negative Rac (N17-Rac) severely impaired serum-induced cyclin D1 mRNA and protein expression in wt and Cav1$^{-/-}$ cells (Fig. 4c). Moreover, cyclin D1 expression in Cav1$^{-/-}$ cells was also reduced at G_0, indicating that Rac activity is required for cyclin D1 accumulation. N17-Rac had no effect on serum-dependent Erk phosphorylation in synchronized wt and Cav1$^{-/-}$ cultures (Fig. 4d), confirming that Rac activation mediates cyclin D1 accumulation in Cav1-deficient cells by a mechanism independent of Erk phosphorylation.

Cav1-deficient cells show AIG. To test the capacity of Cav1-deficient cells for AIG, we seeded MEFs or TFs in soft agar. Both types of Cav1$^{-/-}$ fibroblasts formed colonies (Fig. 5a). Reexpression of Cav1 reverted the phenotype, impairing colony formation by nearly 80% (Fig. 5a), confirming that caveolin deficiency conferred the ability to escape from anchorage dependency and suggesting that it could be an important step in the acquisition of the transformed phenotype. To analyze cell cycle progression of nonadhered cells, we cultured cells overnight on top of a thin layer of agar. Under these conditions 75% ± 0.8% of wt MEFs exited the cell cycle and arrested at G_0/G_1 (Fig. 5b, left), similar to the effect of serum starvation in adhered cultures (Fig. 3a). In contrast, in Cav1$^{-/-}$ MEFs the G_0/G_1 fraction was only 60% ± 1.77%, and this was accompanied by larger S and G_2/M fractions. This increase in the proliferating populations in suspension was analyzed in MEFs-R and -D (15, 44) as well as in cells subjected to RNAi-mediated Cav1 knockdown (Fig. 5b, left). In an alternative approach, wt and Cav1$^{-/-}$ MEFs-R were grown for 16 h in methylcellulose-containing medium under constant rotation. The dividing population was determined by measuring BrdU incorporation during S phase. The proportion of BrdU-positive Cav1$^{-/-}$ cells was approximately eightfold higher than that of wt cells (Fig. 5b, right). G_0 arrest in wt nonadhered MEFs was accompanied by low levels of cyclins D1 and A, which correlated with accumulation of hypophosphorylated pRb (Fig. 5c). In contrast Cav1$^{-/-}$ cells retained higher levels of both cyclins (Fig. 5c) and increased accumulation of nuclear cyclin D1 (Fig. 5d). Similar results were obtained with the three different knockout mice models (MEFs-R and -D and TFs) and in RNAi-silenced Cav1 cells (Fig. 5c and data not shown). Also similar to adherent cultures, Cav1$^{-/-}$ cells showed lower levels of total pRb and p130 protein and higher expression of p107 than the wt. Reexpression of Cav1 in Cav1$^{-/-}$ MEFs recovered the expression levels of cyclins and pocket proteins detected in wt

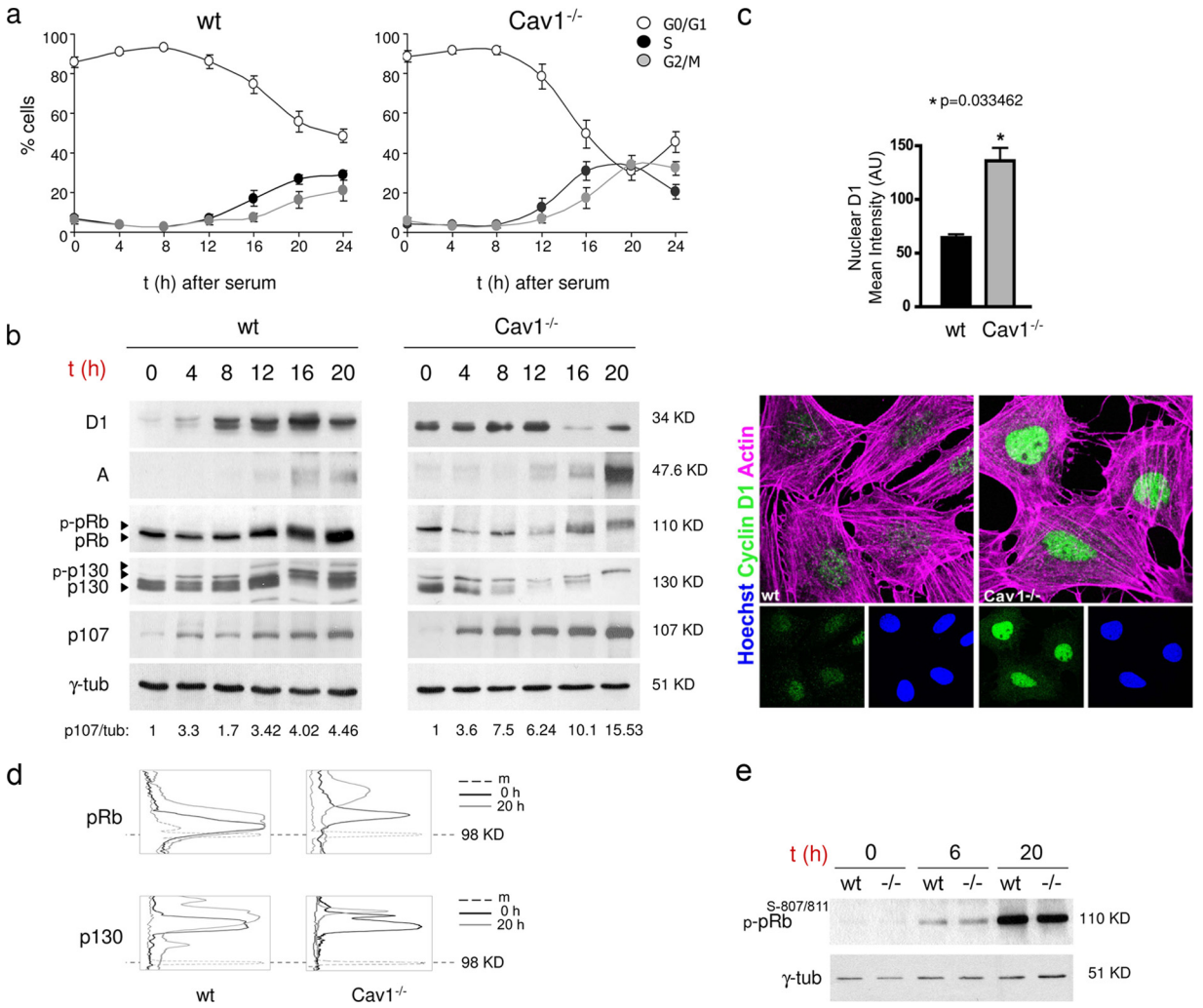

FIG. 3. Faster progression through G_1 and entry into S phase in Cav1$^{-/-}$ MEFs. (a) Flow cytometric analysis of synchronized wt and Cav1$^{-/-}$ MEF-R populations at the indicated times after serum stimulation. Graphs show the percentages of cells in each phase of the cell cycle out of a total of 10,000 cells. (b) Western blot analysis of wt and Cav1$^{-/-}$ MEFs-R after serum stimulation at the indicated time points using antibodies against cyclin D1, cyclin A, pRb, p107, p130, and γ-tubulin (γ-tub; as a loading control). Densitometric analysis of p107 expression normalized to γ-tubulin is indicated (arbitrary units). (c) Immunofluorescence staining of G_0-synchronized populations of wt and Cav1$^{-/-}$ MEFs-R using antibodies against cyclin D1 and phalloidin to visualize the actin cytoskeleton and accumulation of nuclear cyclin D1. At least 30 cells per genotype were analyzed. AU, arbitrary units. (d) Electrophoretic mobility of pRb and p130 proteins compared to a molecular size standard (m) in wt and Cav1$^{-/-}$ MEFs-R at the indicated times after serum stimulation. (e) Western blot analysis of p-pRb (pS807/811) in wt and Cav1$^{-/-}$ MEFs-R at the indicated times after serum stimulation; γ-tubulin was used as a loading control. Bars (a and c) represent means ± standard errors of the means of three independent experiments.

cells in suspension (Fig. 5e). Cav1 reexpression in M21L melanoma cells resulted in a decreased proliferation in suspension (Fig. 5f) and a reduction in cyclin D1 levels as well (not shown). All these data indicate that Cav1$^{-/-}$ cells are able to grow in the absence of adherence to substrate. This phenotype was not influenced by G_1 inhibitors of the CIP/KIP family, since the expression of these factors did not differ significantly between wt and Cav1$^{-/-}$ MEFs, whether under adherent or nonadherent growth conditions (not shown).

AIG in Cav1-deficient cells is Erk independent and Rac activation dependent and involves PI3K and GSK3β. We next examined the signaling pathways underlying adherence-independent growth by Cav1$^{-/-}$ cells. Ras-MAPK, Rac-PAK, and PI3K-Akt were good candidates since all of them are activated in suspended Cav1$^{-/-}$ cells due to defective CEMM internalization after detachment from the ECM (10). We first checked MAPK signaling, due to its importance for integrin-regulated cell cycle progression; however, specific inhibition of Erk phosphorylation in suspended Cav1$^{-/-}$ cells did not interfere with cyclin D1 or A expression or cell cycle progression (Fig. 6a), indicating that this pathway is unrelated to Cav1-mediated control of anchorage. Cyclin D1 is also regulated by PI3K/Akt through the inhibition of GSK3β, a negative regulator of cyclin D1 expression and nuclear accumulation (13). Detached Cav1$^{-/-}$ MEFs showed hyperactivation of the PI3K/Akt pathway (Fig. 6b) (10, 42), and increased Akt phosphorylation has been shown to be Rac dependent in Cav1 knockdown cells (23). Specific inhibition of PI3K with LY294002 decreased

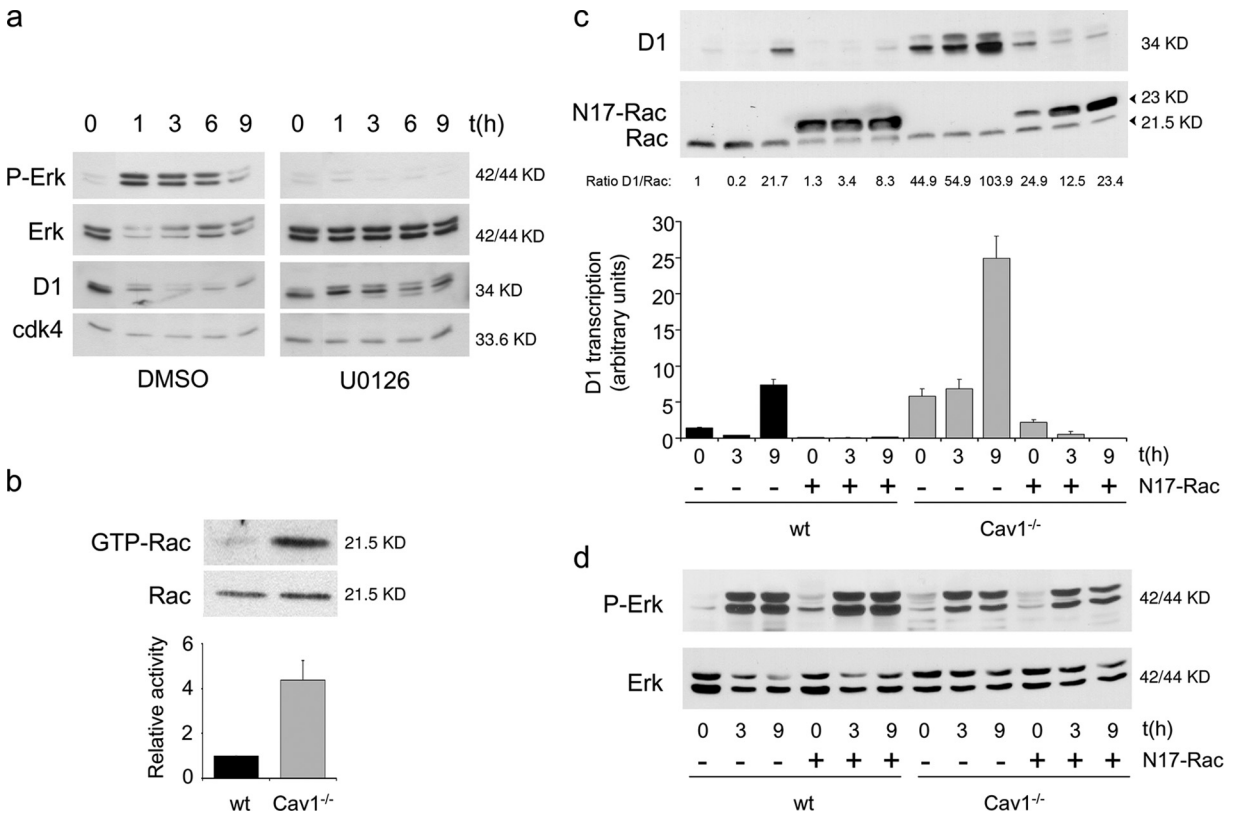

FIG. 4. Rac1 but not Erk induces cyclin D1 in synchronized Cav1$^{-/-}$ MEFs. (a) Western blot analysis of Cav1$^{-/-}$ MEFs using antibodies against the phosphorylated form of Erk (P-Erk), total Erk protein, cyclin D1, and cdk4 (as a loading control) at the indicated times after serum stimulation and in the presence or absence of the specific inhibitor of the p42/44 MAPK pathway, U0126 (10 μM). (b) Rac1 pulldown assay of G_0-synchronized wt and Cav1$^{-/-}$ MEFs after serum starvation. Proteins bound to GST-p21 binding domain were immunoblotted with an antibody against Rac. Densitometric analysis of the relative activity of Rac1 normalized for whole-cell lysates was performed, and the result is expressed as the ratio to activity in wt MEFs. Bar, mean ± standard error of the mean of four independent experiments. (c) Western blot analysis of wt and Cav1$^{-/-}$ MEFs after serum stimulation at the indicated time points using antibodies against cyclin D1 and Rac1, with or without infection of adenovirus N17-Rac. Densitometric analysis of cyclin D1 expression normalized to endogenous Rac is indicated (arbitrary units). qPCR for cyclin D1 mRNA in the same samples was performed. Bars, means ± standard deviations of three experiments. (d) Western blot analysis of wt and Cav1$^{-/-}$ MEFs as in panel c using antibodies against the phosphorylated form of Erk and total Erk protein.

cyclins D1 and A in nonadhered Cav1$^{-/-}$ cells, correlating with an increase in the G_0/G_1 fraction (from 53% ± 2.6% to 68.09% ± 2.69%) and a decrease of S and G_2/M (Fig. 6c). Cyclin expression and cell cycle progression in wt cells were not affected by LY294002 since these cells were already arrested in suspension. Inhibition of GSK3β with LiCl resulted in increased cyclins D1 and A in detached wt cells (Fig. 6c), which correlated with a pronounced reduction in the G_0 population (from 74.92% ± 0.55% to 38.80% ± 2.13%) and increased the S and G_2/M fractions (Fig. 6c). Similar to the data obtained with the pharmacological inhibitors LiCl and LY294002, specific knockdown of GSK3β in wt cells led to cyclin D1 induction in suspension, whereas specific Akt silencing in Cav1$^{-/-}$ MEFs decreased the levels of cyclin D1 (Fig. 6d). Thus, the PI3K/Akt/GSK3β pathway seems to play a determining role in the control of adhesion-dependent proliferation.

In adherent cultures, Rac activity was critical to cyclin D1 expression in Cav1$^{-/-}$ cells (Fig. 4c). In addition, levels of cyclin D1 were increased by expression of constitutively active Rac (V12-Rac) in nonadhered wt Rat1 fibroblasts (Fig. 7a). V12-Rac also reduced the accumulation of nonadhered cells in G_0/G_1 (Fig. 7b). Conversely, the elevated expression of cyclins D1 and A in suspended Cav1$^{-/-}$ MEFs was reduced to wt levels by expression of dominant-negative Rac (Fig. 7c). Rac inhibition in suspended Cav1$^{-/-}$ cells also recovered G_0/G_1 accumulation to nearly wt levels (Fig. 7d). The reduction in the G_0/G_1 fraction of wt and Cav1$^{-/-}$ cells in suspension with the empty vector was a secondary effect of the electroporation and was consistently observed in all experiments. Similarly, suppression of Rac1 expression in suspended Cav1$^{-/-}$ cells by RNAi-mediated silencing resulted in a sharp drop in cyclins D1 and A (Fig. 7e). Thus, Rac activation in detached cells is necessary and sufficient to drive cyclin D1 accumulation and cell cycle progression.

Impaired membrane trafficking and constitutive CEMM/Rac association with the plasma membrane drive cell cycle progression upon loss of integrin-mediated adhesion. CEMM internalization upon loss of anchorage is mediated by caveolae, stable membrane domains that act as vesicular transporters (53). Preincubation of wt cells with latex beads coated with CTxB prevented internalization of CEMMs upon loss of anchorage as described previously (9), a phenotype that resem-

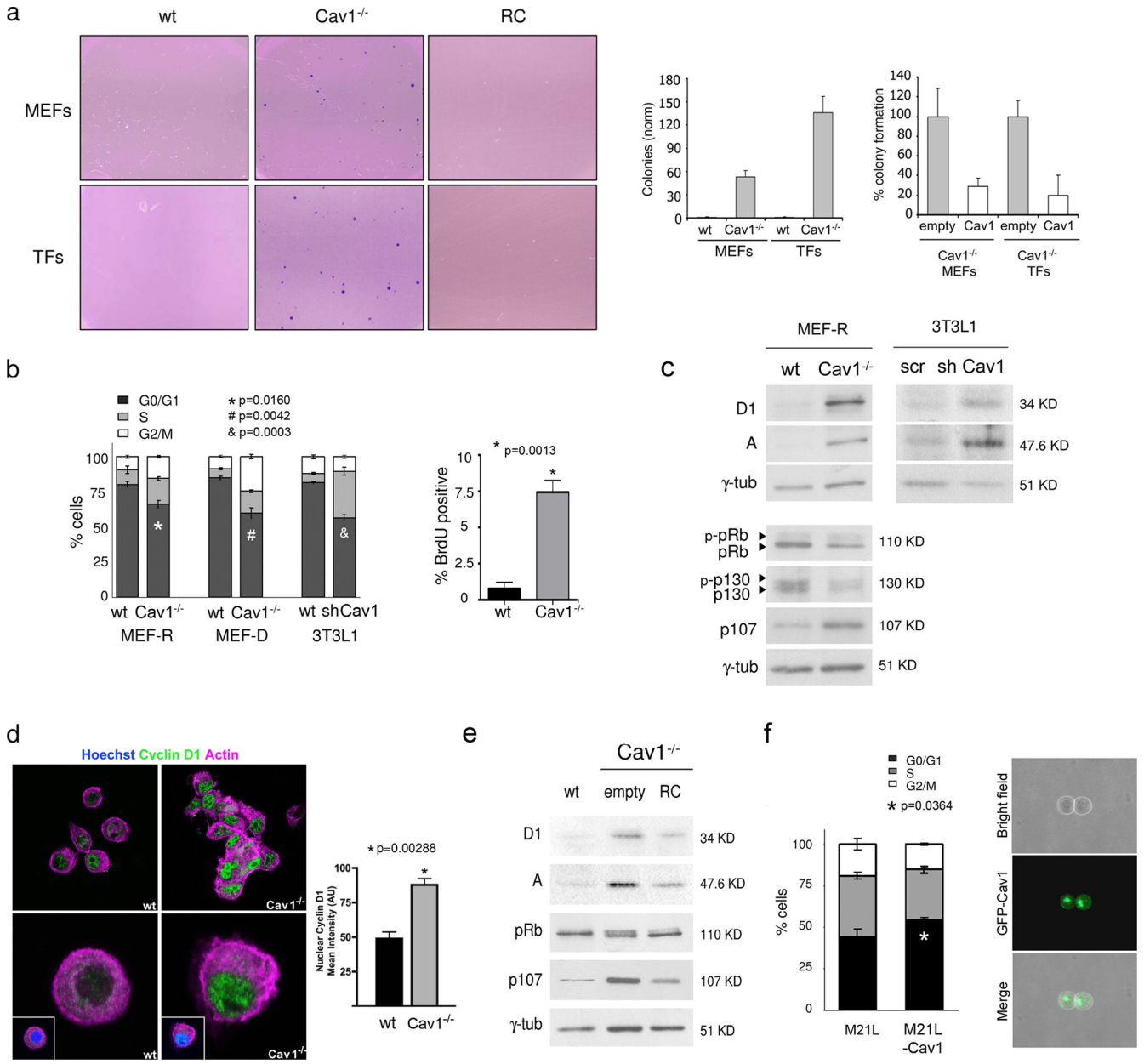

FIG. 5. Cav1$^{-/-}$ fibroblasts show AIG. (a) Soft agar assay for colony formation of wt and Cav1$^{-/-}$ MEFs, Cav1$^{-/-}$ MEFs reconstituted with Cav1 (RC), and TFs. Colonies were stained with crystal violet and photographed. Shown are numbers of colonies formed in soft agar by wt and Cav1$^{-/-}$ MEFs and TFs (left graph) and percentages of colony formation by RC MEFs and TFs (right graph). Bars represent means ± standard errors of the means [SEM] of at least three independent experiments. (b) Flow cytometry profiles of wt and Cav1$^{-/-}$ MEFs-R and -D and 3T3L1 fibroblasts before and after shRNA-mediated Cav1 knockdown, grown in suspension, showing the percentages of cells in each phase of the cell cycle out of a total of 10,000 cells (left) and analysis of BrdU incorporation after 2-h labeling of wt and Cav1$^{-/-}$ MEFs-R cultured in suspension (right). Bars represent means ± SEM of five independent experiments. (c) Western blot analysis of wt and Cav1$^{-/-}$ MEFs-R grown in suspension using antibodies against cyclin D1, cyclin A, pRb, p130, p107, and γ-tubulin (γ-tub; as a loading control) (left) and Western blot analysis of 3T3L1 fibroblasts grown in suspension before and after Cav1 shRNA-mediated specific knockdown using antibodies against cyclin D1, cyclin A and γ-tubulin (as a loading control) (right). (d) Immunofluorescence staining of wt and Cav1$^{-/-}$ MEFs grown in suspension using antibodies against cyclin D1 and phalloidin to visualize the actin cytoskeleton and accumulation of nuclear cyclin D1. Bars represent means ± SEM of three independent experiments after analyzing at least 30 cells per experiment. AU, arbitrary units. (e) Western blot analysis of wt and Cav1$^{-/-}$ MEF-R grown in suspension and expressing either an empty vector or Cav1 (RC) using antibodies against cyclin D1, cyclin A, pRb, p107, and γ-tubulin. Bars represent means ± SEM of four independent experiments. (f) Flow cytometry profiles of M21L melanoma cells grown in suspension and expressing either an empty vector or a construct encoding GFP-fused Cav1, showing the percentages of cells in each phase of the cell cycle out of a total of 10,000 cells (left), and GFP-Cav1 expression in suspended M21L melanoma cells (right).

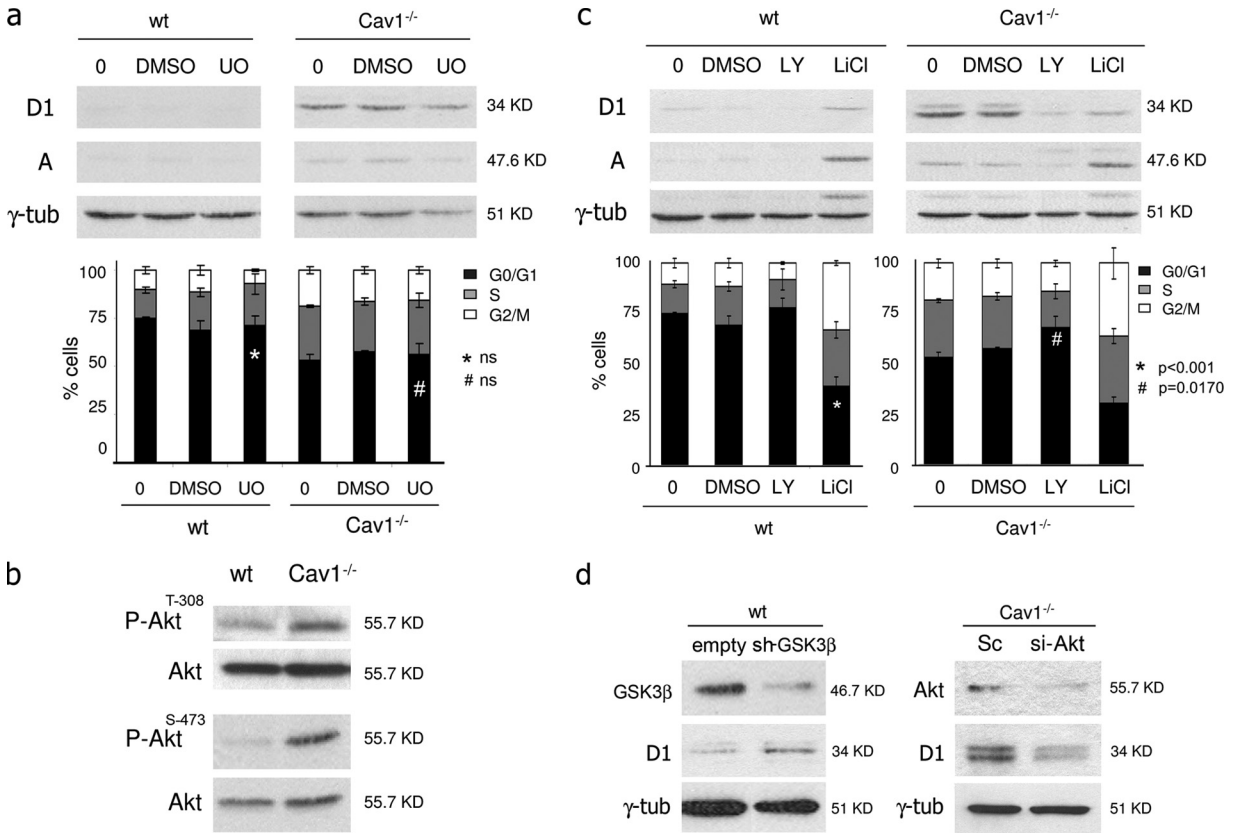

FIG. 6. AIG in Cav1$^{-/-}$ MEFs is mediated by PI3K-GSK3β but not Erk. (a) Western blot analysis of wt and Cav1$^{-/-}$ MEFs grown in suspension in the presence or absence of the MEK inhibitor U0126 using antibodies against cyclin D1, cyclin A, and γ-tubulin (γ-tub; as a loading control) and flow cytometry profiles of wt and Cav1$^{-/-}$ MEFs under the same conditions showing the percentages of cells in each phase of the cell cycle out of a total of 10,000 cells. (b) Western blot analysis of wt and Cav1$^{-/-}$ MEFs grown in suspension using antibodies against the two phosphorylation sites of Akt required for its full activation (p-Akt pT308 and p-Akt pS473) and total Akt as loading control. (c) Western blot analysis of wt and Cav1$^{-/-}$ MEFs grown in suspension in the presence of dimethyl sulfoxide (DMSO) or the specific inhibitors of PI3K (LY294002) and GSK3β (LiCl) using antibodies against cyclin D1, cyclin A, and γ-tubulin (as a loading control) and flow cytometry profiles of wt and Cav1$^{-/-}$ MEFs under the same conditions showing the percentages of cells in each phase of the cell cycle out of a total of 10,000 cells. (d) Western blot analysis of wt and Cav1$^{-/-}$ MEFs grown in suspension after shRNA-mediated knockdown of GSK3β (left) or Akt (right) using antibodies against GSK3β, Akt, cyclin D1, and γ-tubulin. Bars (a and c) represent means ± standard errors of the means of three independent experiments.

bles the Cav1$^{-/-}$ phenotype. The CTxB-treated wt cells showed an almost twofold increase in BrdU incorporation compared with cells treated with uncoated beads or beads coated with an antibody against the TfR, which is excluded from CEMMs (Fig. 8a). This increase in BrdU incorporation correlated with an increase in expression of D1 cyclin in suspension (Fig. 8a). The numbers of beads bound per cell were similar (6.4 ± 2.3 for TfR-coated beads and 7.3 ± 2.8 for CTxB-coated beads), excluding the possibility of an effect on proliferation of bead attachment. Thus, impaired internalization of CEMMs from the plasma membrane induces cell cycle progression in detached cells.

Next we analyzed the effect of constitutive targeting of Rac to the plasma membrane. MEFs were transfected with constructs containing the Rac sequence fused either to the transmembrane region of the IL-2 receptor (IL-2–Rac) or to the myristoylation sequence of Src (myr-Rac). Both Rac mutants produced increased association with the plasma membrane (11) (Fig. 8b). Detached wt MEFs expressing either construct upregulated cyclin D1 and A by two- to threefold (Fig. 8c), and this was accompanied by a reduction in the fraction of cells in G_0 (Fig. 8d). These data suggest that enhanced Rac activation and plasma membrane targeting can account for the increased proliferation and cyclin D1 expression observed in Cav1$^{-/-}$ cells, impairing cell cycle arrest after serum starvation or loss of adhesion. The GTPase Rho has been shown to repress cyclin D1 expression in G_0 and early G_1 (59), thus counteracting the Rac-mediated induction. Interestingly, we have shown that active (GTP-bound) Rho is reduced by nearly 75% in Cav1$^{-/-}$ MEFs (25). Since Rho and Rac activities are mutually antagonistic (4, 25, 59), we analyzed the effect of restoring Rho activity in Cav1$^{-/-}$ cells by expressing a constitutively active Rho mutant (V14-Rho). Rho activity potently downregulated cyclin D1 expression in Cav1$^{-/-}$ cells after either serum starvation (Fig. 9a) or loss of adhesion (Fig. 9b), further supporting the important role of Rac in the hyperproliferative phenotype of Cav1-deficient cells.

DISCUSSION

Our results indicate that in the absence of Cav1 cells are unable to internalize cholesterol-rich domains containing Rac,

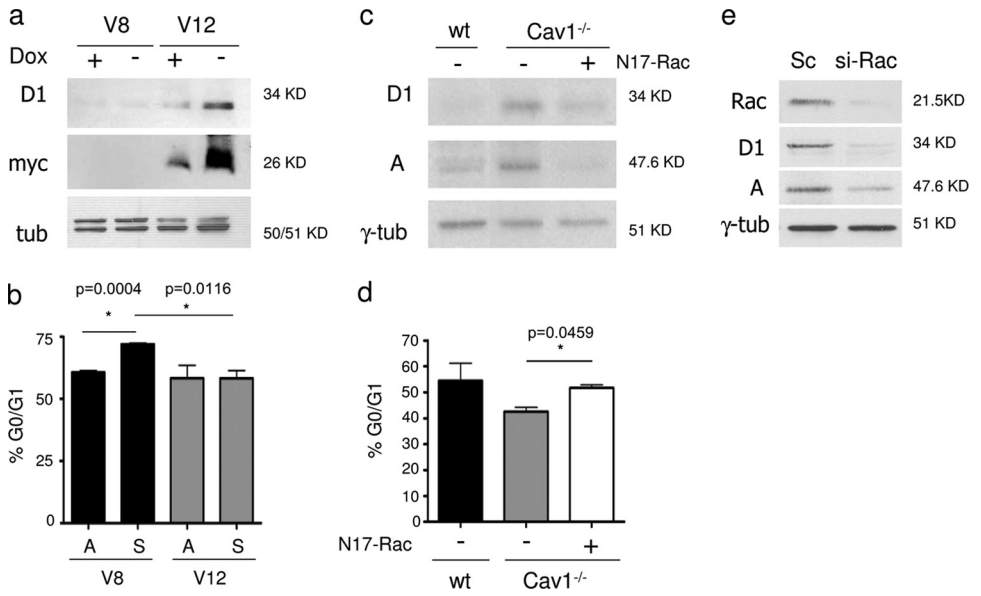

FIG. 7. Rac activation drives cell cycle progression and AIG. (a) Western blot analysis of Rat1 fibroblasts grown in suspension expressing a constitutively active form of Rac (V12) under the control of a tetracycline-responsive promoter or an empty vector (V8) in the presence or absence of doxycycline using antibodies against cyclin D1 and the myc epitope to detect the induction of V12-Rac expression and against γ-tubulin (tub) as a loading control. (b) G_0/G_1 populations of Rat1-V8 and Rat1-V12 cultured under adhesion conditions or in suspension for 48 h in the absence of doxycycline, as determined by flow cytometry out of a total of 10,000 cells. Bars represent means ± standard errors of the means (SEM) of three independent experiments. (c) Western blot analysis of wt and $Cav1^{-/-}$ MEFs in suspension, expressing a dominant negative form of Rac (N17-Rac) or an empty vector, using antibodies against cyclin D1, cyclin A, and γ-tubulin (γ-tub). (d) G_0/G_1 populations of wt and $Cav1^{-/-}$ MEFs grown in suspension, expressing a dominant negative form of Rac (N17-Rac) or an empty vector, as determined by flow cytometry out of a total of 10,000 cells. Bars represent means ± SEM of two independent experiments. (e) Western blot analysis of suspension cultures of $Cav1^{-/-}$ MEFs transfected with an RNAi oligonucleotide directed against Rac1 or with a scramble siRNA, using antibodies against Rac1, cyclin D1, cyclin A, and γ-tubulin.

whose increased activity favors proliferation and bypasses anchorage dependence of growth. Cav1 thus plays a critical role in the induction of cell cycle arrest triggered by lack of nutrients or loss of attachment to the ECM.

Cav1 expression is downregulated or mutated in many human tumors, which suggests that it acts as a tumor suppressor; however, in some organs such as prostate or in certain types of lung cancers it appears to act as a tumor promoter (22, 47). Our results show that Cav1 deficiency, produced by either gene targeting, RNAi-mediated silencing, or oncogene-driven transcriptional downregulation, promotes proliferation, mainly by allowing nuclear accumulation of cyclin D1 in the absence of stimuli from growth factors or integrins. Transcriptional upregulation of cyclin D1 by growth factors is driven by the Erk pathway, and it has been proposed that this pathway contributes to tumorigenesis in several models of Cav1 depletion (20, 48, 62). However, our results show that the Erk pathway is not important for cyclin D1 accumulation or the proliferative phenotype of $Cav1^{-/-}$ cells; both are instead mediated by enhanced Rac activity. Integrin-driven Rac activation can promote the nuclear translocation of Erk (29), so the fact that Erk phosphorylation was not affected by Rac inhibition does not in itself exclude a role for Erk signaling. However, specific inhibition of Erk phosphorylation with U0126 revealed that Erk activation is unnecessary for cyclin D1 accumulation in $Cav1^{-/-}$ cells.

Together with increased cyclin D1 expression, we have observed a general unbalance in the levels of the three members of the pocket protein family (pRb, p130, and p107) in $Cav1^{-/-}$ MEFs. Whereas the role of pRb in G_1 of binding to the S-phase-promoting transcription factors E2F-1, -2, and -3a is well established (58), less is known about the regulatory mechanisms exerted by p130 and p107. Both proteins bind to factors E2F-4 and -5, which are transcriptional repressors. In G_0 and early G_1, p130-E2F complexes at high levels cooperate with pRb-E2F in inhibiting transcription from the target promoters, but the levels of p130 are downregulated in mid- to late G_1, after the protein is hyperphosphorylated. This relieves repression from the promoters and allows binding of transcriptional activators released by hyperphosphorylated pRb (8, 51). p107, however, accumulates as the cell progresses through the cell cycle, correlative to its phosphorylation (3, 6, 32). Whether this accumulation is the result of a phosphorylation-dependent stabilization of the proteins remains to be determined. At this point we cannot determine whether the relatively smaller amounts of pRb and p130 in $Cav1^{-/-}$ MEFs, together with increased accumulation of p107, are the result of increased cyclin D1, but this will certainly be the subject of future studies. We observed that $Cav1^{-/-}$ MEFs arrest at G_0 to the same extent as wt cells and that the timing of G_0 exit and that of pRb phosphorylation are the same in both genotypes. Nonetheless, we postulate that the decreased levels of total pRb protein in $Cav1^{-/-}$ cells promote progression through the G_1 phase of the cell cycle, independently of the phosphorylation rate. The decrease in p130 and increase in p107 might be the result of a hyperphosphorylation of these proteins, as explained above.

Some previous observations have pointed to a role for Cav1 in anchorage dependency regulation, but a direct link has not

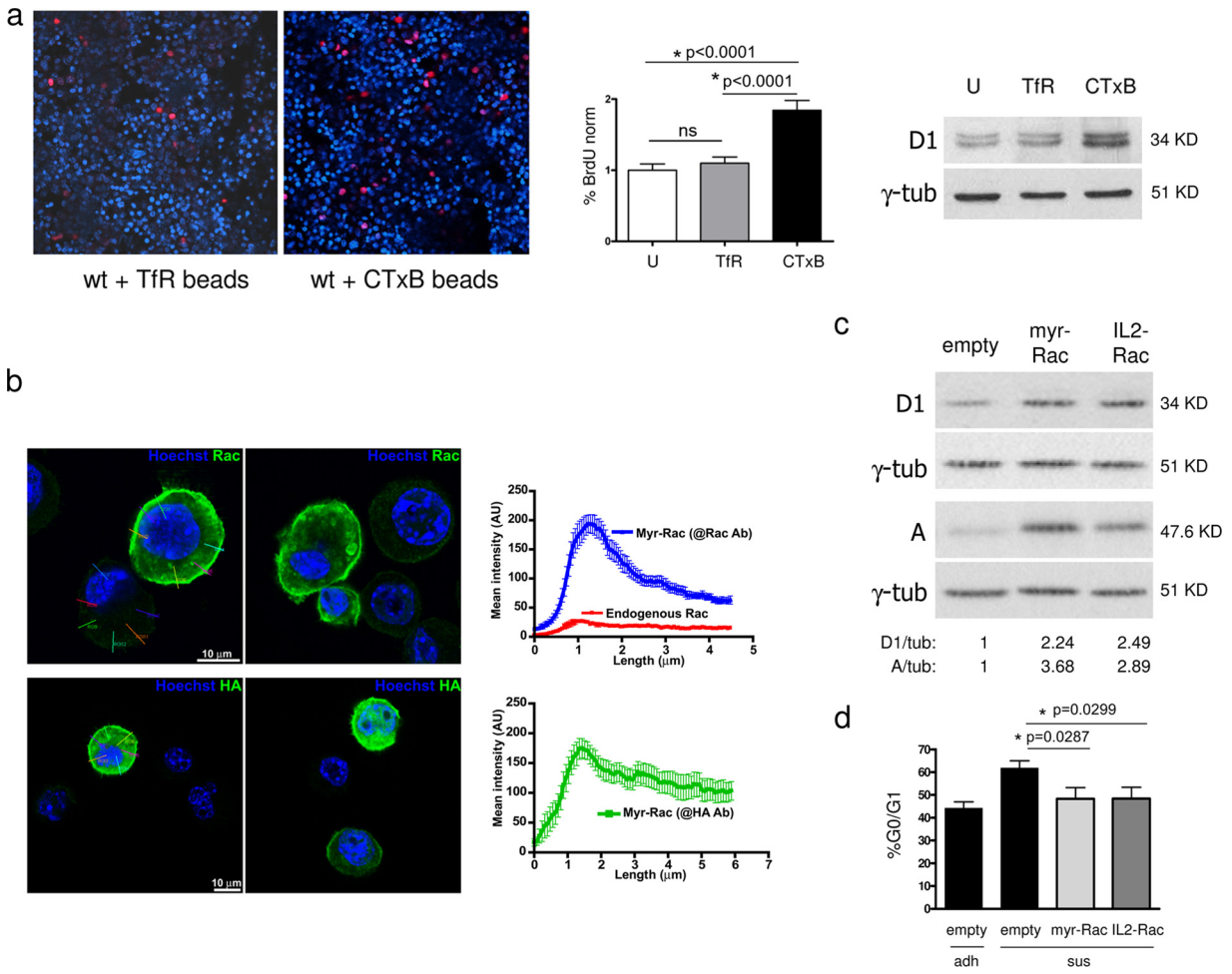

FIG. 8. CEMM/Rac plasma membrane targeting drives cell cycle progression and AIG. (a, left and center) Analysis of BrdU incorporation by immunofluorescence of suspension cultures of wt MEFs after incubation with latex beads either uncoated (U) or coated with CTxB or antibody against TfR. Percentages of BrdU-positive cells are represented. (Right) Western blot analysis of wt MEFs treated as above using antibodies against cyclin D1 and γ-tubulin (γ-tub). Bars represent means ± standard errors of the means (SEM) of two experiments, counting at least 5,000 cells per condition. (b) Immunofluorescence staining of wt MEFs grown in suspension and expressing the membrane-constitutive Rac1 fusion protein myr-HA-Rac using antibodies against Rac1 (top) and HA (bottom), together with Hoechst for nuclear staining. This construct shows enhanced plasma membrane association compared to endogenous Rac. The mean intensity distribution is plotted. AU, arbitrary units. Bars represent means ± SEM of three independent experiments. At least 30 cells per experiment were analyzed. (c) Western blot analysis of wt MEFs grown in suspension and expressing membrane-constitutive Rac1 fusion proteins (myr-HA-Rac or IL-2–HA–Rac) or an empty vector. Antibodies against cyclin D1, cyclin A, and γ-tubulin were used. Results of a densitometric analysis of cyclin D1 and A expression normalized to γ-tubulin are indicated (arbitrary units). (d) G_0/G_1 populations of cells as in panel c, determined by flow cytometry, are represented. Bars represent means ± SEM of five experiments.

been yet established. Some tumors overexpress Cav1, and this expression also correlates with metastasis (22, 55). Other studies with tumor-derived cells or with NIH 3T3 cells transformed with oncogenes (such as v-*src*, v-*abl*, *Bcr-abl*, or *Ras*) show that transformation correlates with a downregulation of Cav1 mRNA and protein expression and that restoration of Cav1 reverses AIG in such tumors (16, 34, 35, 60, 65). Cav1 antisense inhibition in NIH 3T3 confers on the cells the ability to grow in soft agar (20). Our previous work showed that integrins influence Rac-GTPase activation mainly by regulating plasma membrane targeting rather than GTP loading (11). The elevated plasma membrane localization of Rac in Cav1-deficient cells (10) thus suggests that the mechanism by which Cav1 normally suppresses cell growth under the control of integrins might be internalization of Rac-containing liquid-ordered, cholesterol-rich microdomains from the plasma membrane. This internalization would influence many adhesion-dependent growth-regulatory pathways, including Ras-MAPK, Rac-PAK, and PI3K-Akt (Fig. 10). Caveolae are the "internalization vehicle" for these signaling platforms (53). Therefore, Cav1 deficiency leads to disconnection of integrins from such signals and hence defective termination of growth-promoting signaling after loss of adhesion (Fig. 10). CEMM internalization triggered by ECM detachment is a general process that might be relevant to the cessation of proliferation in situations such as invasion, but CEMM internalization mediated by Cav1 might also take place in physiological situations such as mitosis. During the transition from prophase to metaphase, adher-

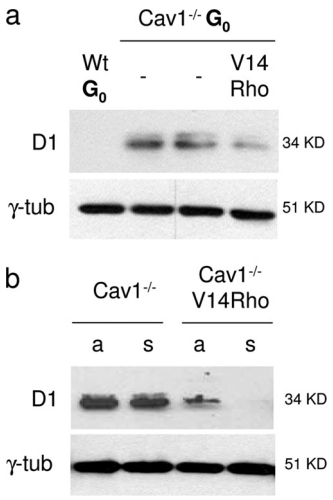

FIG. 9. Rescue of Rho-GTP loading restores cyclin D1 downregulation in both G_0-arrested and suspended Cav1$^{-/-}$ MEFs. Shown is a Western blot analysis of wt and Cav1$^{-/-}$ MEFs with or without expression of a constitutively active form of RhoA (V14-Rho). Cav1$^{-/-}$ MEFs were either serum starved for 72 h (a) or grown under adhesion conditions or in suspension (b). Antibodies against cyclin D1 and γ-tubulin (γ-tub) were used.

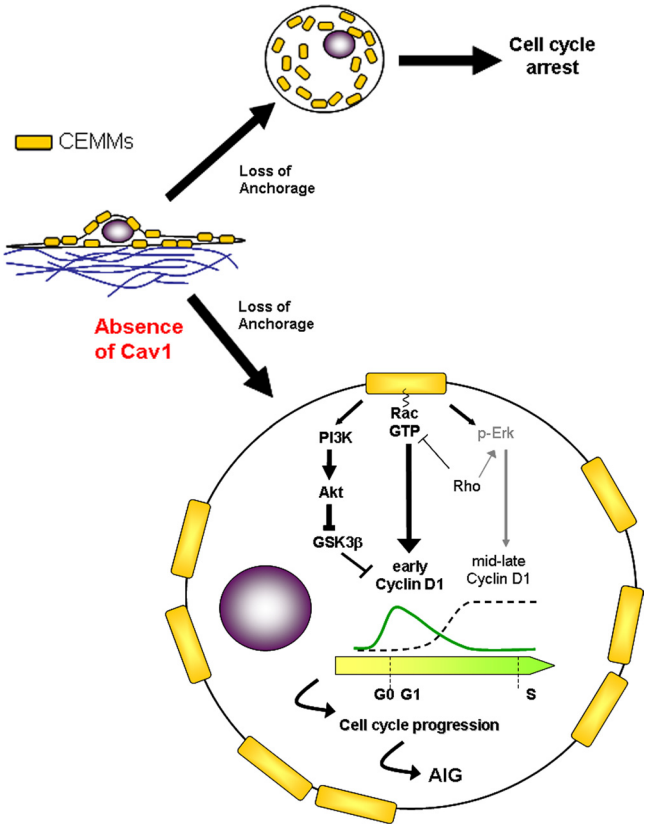

FIG. 10. As a working hypothesis, upon cell detachment from the ECM, Cav1-mediates CEMM endocytosis, leading to the shutdown of several signaling cascades and subsequent cell cycle arrest. In the absence of Cav1, CEMMs cannot be internalized from the plasma membrane, allowing the activation of the Rac, PI3K/Akt, and Erk pathways. On the other hand, absence of Cav1 downregulates Rho activity, which is necessary for Erk effects on cyclin D1 expression and for antagonizing Rac-dependent early cyclin D1 induction. The result is an altered timing of cyclin D1 expression, allowing cell cycle progression in anchorage-independent conditions. Therefore, normal anchorage dependence of growth is regulated by inactivation of adhesive signals upon internalization of CEMMs, which is mediated by Cav1 transport function.

ent cells disrupt their connections to the ECM, consequently rounding up and nearly detaching. This correlates with a large-scale relocation of Cav1 from the plasma membrane to an intracellular compartment, followed by recycling to the cell surface during cytokinesis (R. G. Parton, personal communication).

We have shown here that Cav1$^{-/-}$ cells lose their anchorage independency when Rac activity is abrogated. More importantly, our results indicate that lack of CEMM internalization or forced Rac plasma membrane targeting is sufficient to drive proliferation of wt cells in the absence of substrate anchorage. Our results indicate that, in addition to Rac, another important integrin-regulated pathway, PI3K/Akt/GSK3β, could mediate cyclin D1 accumulation (Fig. 10). By targeting β-catenin for degradation, GSK3β affects cyclin D1 transcription, and GSK3β-mediated cyclin D1 phosphorylation triggers nuclear export and degradation of cyclin D1 during the S phase of the cell cycle (13, 14, 54). We have observed a hyperactivation of PI3K/Akt in Cav1$^{-/-}$ cells, which might drive inactivation of the cyclin D1 inhibitor GSK3β. It is also worth noting that cyclin D1 accumulation in Cav1$^{-/-}$ cells was mainly nuclear. Several previous studies have emphasized the relevance of proper cyclin D1 nuclear export for degradation in S phase, and nonexportable cyclin D1 mutants are highly transforming independently of other cooperating oncogenes (21). We have indeed observed degradation of cyclin D1 in Cav1$^{-/-}$ MEFs in S phase, thus indicating that the nuclear export of this protein is not fully impaired but is probably less efficient than in wt cells. This would be in agreement with a reduced GSK3β-associated activity as the result of the PI3K/Akt hyperactivation observed.

The Erk pathway is a key regulator of cell cycle progression (1) and is frequently hyperactivated in the absence of Cav1, for example, after Cav1 antisense inhibition (20); in genetic models producing Cav1 deficiency, including those involving *Caenorhabditis elegans* (48); and in tissues and organs of Cav1$^{-/-}$ mice (36, 62). Moreover, integrin-regulated Cav1-mediated CEMM internalization is known to affect Erk signaling in addition to Rac and PI3K/Akt (10). The absence of regulation by Erk in our studies is difficult to reconcile with previous results. The explanation may lie in the defective Rho-GTP loading in Cav1$^{-/-}$ cells, since Rho controls the "normal" timing of cyclin D1 expression in mid-G_1 by allowing sustained Erk activation (59). Rho downregulation in the absence of Cav1 would render ineffective the general Erk hyperactivation in terms of cell cycle regulation. Moreover, Rho antagonizes the Rac-dependent expression of cyclin D1 at G_0 and early G_1 (Fig. 10). This mirrors the phenotype of Cav1$^{-/-}$ cells and parallels the restoration of normal-pattern cyclin D1 expression with a constitutively active Rho mutant in serum-starved and nonadhered Cav1$^{-/-}$ cells.

Thus, abnormal cyclin D1 expression, hyperproliferation, and AIG upon loss of Cav1 result from the combined effects of

Rho downregulation, Rac hyperactivation (which is fivefold higher at G_0 in Cav1$^{-/-}$ cells than in wt cells), and increased Rac membrane targeting. Rac membrane targeting and hyperactivation drive cyclin D1 expression by an Erk-independent mechanism, and the PI3K/Akt/GSK3β pathway might mediate Rac effects (Fig. 10). This concurs with the finding that increased Akt phosphorylation induced by RNAi-mediated knockdown of Cav1 is Rac dependent (23). The observation that G_0 arrest and exit are unaltered in Cav1$^{-/-}$ MEFs indicates that the increased cyclin D1 at G_0 does not increase cdk4/6 activity. One possible explanation is that inhibitors of the INK family (reviewed in reference 50) counteract the excess cyclin D1 expression at G_0 and prevent cdk4/6 activity and thus early pRb phosphorylation. The analysis of other critical regulators of the G_1-to-S-phase transition, such as the inhibitors of the CIP/KIP family (which are upregulated after deprivation of either growth factor or adhesion signals) did not reveal alterations in the Cav1$^{-/-}$ MEFs (not shown). This excludes the possibility that the phenotype observed could be in part the result of an insufficient induction of those inhibitors. Instead, this suggests that the increase in cyclin D1 is sufficient to bypass the subsequent control of cyclin E-associated activity, thereby shortening G_1 and allowing cells to enter S phase; this would strengthen the link between cyclin D1 expression and cell cycle progression in the absence of Cav1. In agreement, cyclin D1 downregulation after Rac inhibition or GSK3β reactivation results in cell cycle arrest in Cav1$^{-/-}$ cells, as had been already reported for other systems (57).

AIG is a major characteristic of cell transformation and is the in vitro characteristic that best correlates with tumorigenesis in vivo (18). The results presented here thus provide novel insight into the mechanisms that regulate cell cycle progression and AIG in those tumor cells which have lost caveolin function.

ACKNOWLEDGMENTS

We thank Michael P. Lisanti for MEFs-R, Lucas Pelkmans and Teymuras Kurzchalia for MEFs-D, and Richard G. W. Anderson for TFs from Cav1$^{-/-}$ and Cav1$^{+/+}$ littermate mice. We thank M. Camps and A. Pol for Cav1-silenced 3T3L1 fibroblasts, Anne Ridley for N17-Rac adenovirus, Marc Symons for Rat1-V12Rac cells, and M. Barbacid and A. C. Carrera for antibodies. We thank D. Turner for GSK3β shRNA. We thank Nazilla B. Alderson for technical assistance. We are grateful to Miguel R. Campanero and David Santamaría for critical reading of the manuscript. Editorial assistance was provided by Simon Bartlett.

This work was supported by the MICINN (Spanish Ministry of Science and Innovation) through grants SAF2005-00493, GEN2003-20239-C06-04, and RTICC (Cancer Research Network) RD06/0020/1033 to M.A.D.P.; by EUROHORCS (European Heads Of Research Councils) and the European Science Foundation through a EURYI (European Young Investigator) award to M.A.D.P.; by the EMBO Young Investigator Programme; and by the European Union 6th Framework Programme through a Marie Curie International Reintegration Grant (MIRG-CT-2005-016427, to M.A.D.P.). A.C. was supported initially by a postdoctoral Juan de la Cierva Contract (MICINN) and later by the Spanish Cancer Research Association (AECC), M.C.G. was supported by a predoctoral fellowship (BES-2006-13204, MICINN), and J.G.G. was supported by a CNIC postdoctoral contract. E.K. and R.K.A. were supported by NIH grant CA72639. The CNIC is supported by the Institute of Health Carlos III (MICINN) and the Pro-CNIC Foundation.

REFERENCES

1. **Assoian, R. K., and E. A. Klein.** 2008. Growth control by intracellular tension and extracellular stiffness. Trends Cell Biol. **18:**347–352.
2. **Bar-Sagi, D., and A. Hall.** 2000. Ras and Rho GTPases: a family reunion. Cell **103:**227–238.
3. **Beijersbergen, R. L., L. Carlee, R. M. Kerkhoven, and R. Bernards.** 1995. Regulation of the retinoblastoma protein-related p107 by G1 cyclin complexes. Genes Dev. **9:**1340–1353.
4. **Burridge, K., and K. Wennerberg.** 2004. Rho and Rac take center stage. Cell **116:**167–179.
5. **Bustelo, X. R., V. Sauzeau, and I. M. Berenjeno.** 2007. GTP-binding proteins of the Rho/Rac family: regulation, effectors and functions in vivo. Bioessays **29:**356–370.
6. **Classon, M., and N. Dyson.** 2001. p107 and p130: versatile proteins with interesting pockets. Exp. Cell Res. **264:**135–147.
7. **Classon, M., and E. Harlow.** 2002. The retinoblastoma tumour suppressor in development and cancer. Nat. Rev. Cancer **2:**910–917.
8. **Cobrinik, D.** 2005. Pocket proteins and cell cycle control. Oncogene **24:**2796–2809.
9. **del Pozo, M. A., N. B. Alderson, W. B. Kiosses, H. H. Chiang, R. G. Anderson, and M. A. Schwartz.** 2004. Integrins regulate Rac targeting by internalization of membrane domains. Science **303:**839–842.
10. **del Pozo, M. A., N. Balasubramanian, N. B. Alderson, W. B. Kiosses, A. Grande-Garcia, R. G. Anderson, and M. A. Schwartz.** 2005. Phospho-caveolin-1 mediates integrin-regulated membrane domain internalization. Nat. Cell Biol. **7:**901–908.
11. **del Pozo, M. A., L. S. Price, N. B. Alderson, X. D. Ren, and M. A. Schwartz.** 2000. Adhesion to the extracellular matrix regulates the coupling of the small GTPase Rac to its effector PAK. EMBO J. **19:**2008–2014.
12. **del Pozo, M. A., M. Vicente-Manzanares, R. Tejedor, J. M. Serrador, and F. Sánchez-Madrid.** 1999. Rho GTPases control migration and polarization of adhesion molecules and cytoskeletal ERM components in T lymphocytes. Eur. J. Immunol. **29:**3609–3620.
13. **Diehl, J. A., M. Cheng, M. F. Roussel, and C. J. Sherr.** 1998. Glycogen synthase kinase-3beta regulates cyclin D1 proteolysis and subcellular localization. Genes Dev. **12:**3499–3511.
14. **Diehl, J. A., F. Zindy, and C. J. Sherr.** 1997. Inhibition of cyclin D1 phosphorylation on threonine-286 prevents its rapid degradation via the ubiquitin-proteasome pathway. Genes Dev. **11:**957–972.
15. **Drab, M., P. Verkade, M. Elger, M. Kasper, M. Lohn, B. Lauterbach, J. Menne, C. Lindschau, F. Mende, F. C. Luft, A. Schedl, H. Haller, and T. V. Kurzchalia.** 2001. Loss of caveolae, vascular dysfunction, and pulmonary defects in caveolin-1 gene-disrupted mice. Science **293:**2449–2452.
16. **Engelman, J. A., C. C. Wykoff, S. Yasuhara, K. S. Song, T. Okamoto, and M. P. Lisanti.** 1997. Recombinant expression of caveolin-1 in oncogenically transformed cells abrogates anchorage-independent growth. J. Biol. Chem. **272:**16374–16381.
17. **Engelman, J. A., X. L. Zhang, and M. P. Lisanti.** 1998. Genes encoding human caveolin-1 and -2 are co-localized to the D7S522 locus (7q31.1), a known fragile site (FRA7G) that is frequently deleted in human cancers. FEBS Lett. **436:**403–410.
18. **Freedman, V. H., and S. I. Shin.** 1974. Cellular tumorigenicity in nude mice: correlation with cell growth in semi-solid medium. Cell **3:**355–359.
19. **Frisch, S. M., and R. A. Screaton.** 2001. Anoikis mechanisms. Curr. Opin. Cell Biol. **13:**555–562.
20. **Galbiati, F., D. Volonte, J. A. Engelman, G. Watanabe, R. Burk, R. G. Pestell, and M. P. Lisanti.** 1998. Targeted downregulation of caveolin-1 is sufficient to drive cell transformation and hyperactivate the p42/44 MAP kinase cascade. EMBO J. **17:**6633–6648.
21. **Gladden, A. B., and J. A. Diehl.** 2005. Location, location, location: the role of cyclin D1 nuclear localization in cancer. J. Cell. Biochem. **96:**906–913.
22. **Goetz, J. G., P. Lajoie, S. M. Wiseman, and I. R. Nabi.** 2008. Caveolin-1 in tumor progression: the good, the bad and the ugly. Cancer Metastasis Rev. **27:**715–735.
23. **Gonzalez, E., A. Nagiel, A. J. Lin, D. E. Golan, and T. Michel.** 2004. Small interfering RNA-mediated down-regulation of caveolin-1 differentially modulates signaling pathways in endothelial cells. J. Biol. Chem. **279:**40659–40669.
24. **Gonzalez-Munoz, E., C. Lopez-Iglesias, M. Calvo, M. Palacin, A. Zorzano, and M. Camps.** 2009. Caveolin-1 loss-of-function accelerates GLUT4 and insulin receptor degradation in 3T3-L1 adipocytes. Endocrinology **150:**3493–3502.
25. **Grande-García, A., A. Echarri, J. de Rooij, N. B. Alderson, C. M. Waterman-Storer, J. M. Valdivielso, and M. A. del Pozo.** 2007. Caveolin-1 regulates cell polarization and directional migration through Src kinase and Rho GTPases. J. Cell Biol. **177:**683–694.
26. **Han, S. E., K. H. Park, G. Lee, Y. J. Huh, and B. M. Min.** 2004. Mutation and aberrant expression of caveolin-1 in human oral squamous cell carcinomas and oral cancer cell lines. Int. J. Oncol. **24:**435–440.
27. **Hancock, J. F.** 2006. Lipid rafts: contentious only from simplistic standpoints. Nat. Rev. Mol. Cell Biol. **7:**456–462.
28. **Hayashi, K., S. Matsuda, K. Machida, T. Yamamoto, Y. Fukuda, Y. Nimura, T. Hayakawa, and M. Hamaguchi.** 2001. Invasion activating caveolin-1 mutation in human scirrhous breast cancers. Cancer Res. **61:**2361–2364.
29. **Hirsch, E., L. Barberis, M. Brancaccio, O. Azzolino, D. Xu, J. M. Kyriakis,**

L. Silengo, F. G. Giancotti, G. Tarone, R. Fassler, and F. Altruda. 2002. Defective Rac-mediated proliferation and survival after targeted mutation of the beta1 integrin cytodomain. J. Cell Biol. **157:**481–492.
30. **Jacobson, K., O. G. Mouritsen, and R. G. Anderson.** 2007. Lipid rafts: at a crossroad between cell biology and physics. Nat. Cell Biol. **9:**7–14.
31. **Jay, S. M., E. Skokos, F. Laiwalla, M. M. Krady, and T. R. Kyriakides.** 2007. Foreign body giant cell formation is preceded by lamellipodia formation and can be attenuated by inhibition of Rac1 activation. Am. J. Pathol. **171:**632–640.
32. **Kiess, M., R. M. Gill, and P. A. Hamel.** 1995. Expression and activity of the retinoblastoma protein (pRB)-family proteins, p107 and p130, during L6 myoblast differentiation. Cell Growth Differ. **6:**1287–1298.
33. **Klein, E. A., Y. Yung, P. Castagnino, D. Kothapalli, and R. K. Assoian.** 2007. Cell adhesion, cellular tension, and cell cycle control. Methods Enzymol. **426:**155–175.
34. **Koleske, A. J., D. Baltimore, and M. P. Lisanti.** 1995. Reduction of caveolin and caveolae in oncogenically transformed cells. Proc. Natl. Acad. Sci. USA **92:**1381–1385.
35. **Lee, S. W., C. L. Reimer, P. Oh, D. B. Campbell, and J. E. Schnitzer.** 1998. Tumor cell growth inhibition by caveolin re-expression in human breast cancer cells. Oncogene **16:**1391–1397.
36. **Le Lay, S., and T. V. Kurzchalia.** 2005. Getting rid of caveolins: phenotypes of caveolin-deficient animals. Biochim. Biophys. Acta **1746:**322–333.
37. **Li, J., B. A. Ballif, A. M. Powelka, J. Dai, S. P. Gygi, and V. W. Hsu.** 2005. Phosphorylation of ACAP1 by Akt regulates the stimulation-dependent recycling of integrin beta1 to control cell migration. Dev. Cell **9:**663–673.
38. **Martin, K. H., J. K. Slack, S. A. Boerner, C. C. Martin, and J. T. Parsons.** 2002. Integrin connections map: to infinity and beyond. Science **296:**1652–1653.
39. **Martinez-Gac, L., M. Marques, Z. Garcia, M. R. Campanero, and A. C. Carrera.** 2004. Control of cyclin G2 mRNA expression by forkhead transcription factors: novel mechanism for cell cycle control by phosphoinositide 3-kinase and forkhead. Mol. Cell. Biol. **24:**2181–2189.
40. **Mayor, S., and R. E. Pagano.** 2007. Pathways of clathrin-independent endocytosis. Nat. Rev. Mol. Cell Biol. **8:**603–612.
41. **Mettouchi, A., S. Klein, W. Guo, M. Lopez-Lago, E. Lemichez, J. K. Westwick, and F. G. Giancotti.** 2001. Integrin-specific activation of Rac controls progression through the G(1) phase of the cell cycle. Mol. Cell **8:**115–127.
42. **Murata, T., M. I. Lin, Y. Huang, J. Yu, P. M. Bauer, F. J. Giordano, and W. C. Sessa.** 2007. Reexpression of caveolin-1 in endothelium rescues the vascular, cardiac, and pulmonary defects in global caveolin-1 knockout mice. J. Exp. Med. **204:**2373–2382.
43. **Parton, R. G., and K. Simons.** 2007. The multiple faces of caveolae. Nat. Rev. Mol. Cell Biol. **8:**185–194.
44. **Razani, B., J. A. Engelman, X. B. Wang, W. Schubert, X. L. Zhang, C. B. Marks, F. Macaluso, R. G. Russell, M. Li, R. G. Pestell, D. Di Vizio, H. Hou, Jr., B. Kneitz, G. Lagaud, G. J. Christ, W. Edelmann, and M. P. Lisanti.** 2001. Caveolin-1 null mice are viable but show evidence of hyperproliferative and vascular abnormalities. J. Biol. Chem. **276:**38121–38138.
45. **Ridley, A. J.** 2001. Cyclin' round the cell with Rac. Dev. Cell **1:**160–161.
46. **Sahai, E., and C. J. Marshall.** 2002. Rho-GTPases and cancer. Nat. Rev. Cancer **2:**133–142.
47. **Salanueva, I. J., A. Cerezo, M. C. Guadamillas, and M. A. del Pozo.** 2007. Integrin regulation of caveolin function. J. Cell. Mol. Med. **11:**969–980.
48. **Scheel, J., J. Srinivasan, U. Honnert, A. Henske, and T. V. Kurzchalia.** 1999. Involvement of caveolin-1 in meiotic cell-cycle progression in *Caenorhabditis elegans*. Nat. Cell Biol. **1:**127–129.
49. **Schwartz, M. A., and M. H. Ginsberg.** 2002. Networks and crosstalk: integrin signalling spreads. Nat. Cell Biol. **4:**E65–E68.
50. **Sherr, C. J., and J. M. Roberts.** 1999. CDK inhibitors: positive and negative regulators of G1-phase progression. Genes Dev. **13:**1501–1512.
51. **Sun, A., L. Bagella, S. Tutton, G. Romano, and A. Giordano.** 2007. From G0 to S phase: a view of the roles played by the retinoblastoma (Rb) family members in the Rb-E2F pathway. J. Cell. Biochem. **102:**1400–1404.
52. **Sunaga, N., K. Miyajima, M. Suzuki, M. Sato, M. A. White, R. D. Ramirez, J. W. Shay, A. F. Gazdar, and J. D. Minna.** 2004. Different roles for caveolin-1 in the development of non-small cell lung cancer versus small cell lung cancer. Cancer Res. **64:**4277–4285.
53. **Tagawa, A., A. Mezzacasa, A. Hayer, A. Longatti, L. Pelkmans, and A. Helenius.** 2005. Assembly and trafficking of caveolar domains in the cell: caveolae as stable, cargo-triggered, vesicular transporters. J. Cell Biol. **170:**769–779.
54. **Tetsu, O., and F. McCormick.** 1999. Beta-catenin regulates expression of cyclin D1 in colon carcinoma cells. Nature **398:**422–426.
55. **Thompson, T. C., T. L. Timme, L. Li, and A. Goltsov.** 1999. Caveolin-1, a metastasis-related gene that promotes cell survival in prostate cancer. Apoptosis **4:**233–237.
56. **Valasek, M. A., J. Weng, P. W. Shaul, R. G. Anderson, and J. J. Repa.** 2005. Caveolin-1 is not required for murine intestinal cholesterol transport. J. Biol. Chem. **280:**28103–28109.
57. **Villanueva, J., Y. Yung, J. L. Walker, and R. K. Assoian.** 2007. ERK activity and G1 phase progression: identifying dispensable versus essential activities and primary versus secondary targets. Mol. Biol. Cell **18:**1457–1463.
58. **Weinberg, R. A.** 1995. The retinoblastoma protein and cell cycle control. Cell **81:**323–330.
59. **Welsh, C. F., K. Roovers, J. Villanueva, Y. Liu, M. A. Schwartz, and R. K. Assoian.** 2001. Timing of cyclin D1 expression within G1 phase is controlled by Rho. Nat. Cell Biol. **3:**950–957.
60. **Wiechen, K., C. Sers, A. Agoulnik, K. Arlt, M. Dietel, P. M. Schlag, and U. Schneider.** 2001. Down-regulation of caveolin-1, a candidate tumor suppressor gene, in sarcomas. Am. J. Pathol. **158:**833–839.
61. **Williams, T. M., M. W. Cheung, D. S. Park, B. Razani, A. W. Cohen, W. J. Muller, D. Di Vizio, N. G. Chopra, R. G. Pestell, and M. P. Lisanti.** 2003. Loss of caveolin-1 gene expression accelerates the development of dysplastic mammary lesions in tumor-prone transgenic mice. Mol. Biol. Cell **14:**1027–1042.
62. **Williams, T. M., and M. P. Lisanti.** 2005. Caveolin-1 in oncogenic transformation, cancer, and metastasis. Am. J. Physiol. Cell. Physiol. **288:**C494–C506.
63. **Yang, G., T. L. Timme, A. Frolov, T. M. Wheeler, and T. C. Thompson.** 2005. Combined c-Myc and caveolin-1 expression in human prostate carcinoma predicts prostate carcinoma progression. Cancer **103:**1186–1194.
64. **Yu, J. Y., J. Taylor, S. L. DeRuiter, A. B. Vojtek, and D. L. Turner.** 2003. Simultaneous inhibition of GSK3alpha and GSK3beta using hairpin siRNA expression vectors. Mol. Ther. **7:**228–236.
65. **Zhang, W., B. Razani, Y. Altschuler, B. Bouzahzah, K. E. Mostov, R. G. Pestell, and M. P. Lisanti.** 2000. Caveolin-1 inhibits epidermal growth factor-stimulated lamellipod extension and cell migration in metastatic mammary adenocarcinoma cells (MTLn3). Transformation suppressor effects of adenovirus-mediated gene delivery of caveolin-1. J. Biol. Chem. **275:**20717–20725.